Shape Reconstruction and Rotation Axis Estimation of Small Bodies Based on Structure-from-Motion

Huan Xie [1*], Yifan Wang[1], Xiongfeng Yan[1], Ming Yang[1], Yaqiong Wang[1], Xiaohua Tong[1]

[1] College of Surveying and Geo-Informatics, and Shanghai Key Laboratory of Space Mapping and Remote Sensing for Planetary Exploration, Tongji University, Shanghai 200092, China - huanxie@tongji.edu.cn

Keywords: Small bodies, Structure from motion, Shape reconstruction, Rotation axis estimation.

Abstract:

Shape reconstruction and rotation axis estimation of small bodies essential for both engineering applications and scientific investigations. This paper presents a Structure-from-Motion-based (SFM) method for small body shape reconstruction and rotation axis estimation. The method enables fast and autonomous estimation of shape and rotation axis at relatively large distances during the approach phase with a limited number of images. Using near-hovering observations, sequential image poses are estimated via incremental SFM. The normal vector of the plane where the fitted space circle is located is identified as the small body’s rotation axis and transformed into the small body-centered J2000 inertial coordinate system. A global shape model is then generated through dense stereo matching. The proposed method is evaluated using both simulated and real mission data. A total of 75 simulation cases are designed, accounting for sun phase angle, approach angle, small body shape, and image count per rotation period. Results show that over 95% of cases achieve a rotation axis estimation error below 5°. When tens of images are captured per rotation period, the rotation axis can be estimated within minutes. Validation with OSIRIS-REx mission data for Bennu yields a rotation axis estimation error of approximately 1°, while dense reconstruction shows an average deviation of 2.55 m compared to the SPC shape model. These findings demonstrate the method’s effectiveness and suitability for small body exploration.

1. Introduction

The research of small bodies has gradually become one of the key developmental fields in international deep space exploration (Zhang, Xu and Ding, 2021). Shape reconstruction and rotation axis estimation of small bodies are essential for both engineering applications and scientific investigations. From an engineering standpoint, they form the basis for establishing a body-fixed coordinate system, enabling precise navigation and mission planning for sample-return operations. From a scientific perspective, they offer valuable insights into the origin and evolution of small bodies, deepening our understanding of their formation processes and long-term development.

According to the imaging effect of the target small body, existing methods for estimating the rotation axis of small bodies can be classified into three categories: the light curve-based, the silhouette-based and the image feature-based methods. In the early approach phase, when the small body appears as only a few pixels in an image, its brightness variations over time can be used to construct a light curve. This curve depends on the object’s shape, rotation state, and surface scattering properties. The convex inversion method leverages this principle, using least squares fitting to estimate both the convex shape model and rotation axis orientation. While widely applied for long-distance axis estimation (Chamberlain, Sykes and Esquerdo, 2007; Mottola *et al.*, 2014), this method requires images spanning multiple rotation periods at varying sun phase angles and is computationally inefficient (Muinonen *et al.*, 2015). Moreover, its accuracy is limited, making it primarily useful for generating an initial estimate.

As the spacecraft moves closer, the small body’s silhouette becomes distinct against the dark background. The silhouette-based approach reconstructs a shape model using techniques like voxel elimination or ray trimming, then estimates the rotation axis by comparing silhouette similarities between the model and actual images (Bandyopadhyay *et al.*, 2019, 2021). While effective, this method is computationally expensive, requiring an exhaustive search across the celestial sphere. Expanding the search range or refining the step size significantly increases computational cost. Additionally, it performs poorly for small bodies with regular or near-spherical shapes, as their silhouettes remain largely unchanged from different viewing angles (Bandyopadhyay *et al.*, 2021).

Image feature-based methods, such as stereophotogrammetry (SPG) and stereophotoclinometry (SPC), offer the highest accuracy, achieving sub-meter shape reconstruction and rotation axis estimates with uncertainties as low as 10^{-3} degrees (Preusker *et al.*, 2015; Park *et al.*, 2019). However, they require extensive high-resolution imaging over several rotation periods, often spanning months, making them impractical for the approach phase. Additionally, these methods rely on significant human intervention for solution refinement and model validation (Panicucci *et al.*, 2023).

The vision-based systems have been gaining attention as a more cost-effective solution, such as Structure-from-Motion (SFM). To address the challenges posed by limited imaging and weak surface textures during the approach phase of small body exploration, we developed an SFM-based method for shape reconstruction and rotation axis estimation. This method operates autonomously without reliance on ground communications, enabling real-time onboard estimation of rotational properties. Its effectiveness is demonstrated through both simulation data and in-orbit observations of Bennu.

2. Methodology

During the approach phase, as the spacecraft nears the small body, it continuously observes the target over one complete rotation period. Given the long distance, the spacecraft’s relative movement to the small body during this period can be neglected

(approximately a hovering observation). Consequently, the small body’s rotational information can be inferred from the relative motion of the camera. The framework of the proposed method is shown in Figure 1, mainly include four parts: image matching, camera pose estimation, rotation axis estimation and dense reconstruction.

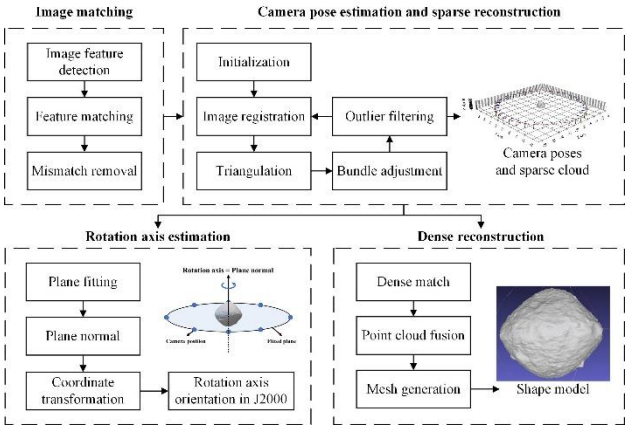

Figure 1. Framework of the proposed method

2.1 Image matching

The first step of the proposed method is image feature point detection and image matching. Common feature detection algorithms include SIFT, SURF, BRISK, ORB, Harris, etc., which differ in the types of structures (e.g., corners, blobs, or edges) and their computational complexity. SIFT feature detection algorithm was adopted because of its scale and rotation invariance, which can stably extract surface feature points of small bodies under the conditions of weak image texture and changing observation conditions (Lowe, 2004).

In this study, the images used were captured during one complete rotation period of the small body. To avoid redundant matches caused by brute-force matching, image pairs were constructed based on the sequence of image acquisition. Specifically, each image was paired with the three adjacent images before and after it. After computing the feature descriptors, FASTCASCADEHASHINGL2, an efficient nearest-neighbour matching method, was employed. This method uses the L2 norm (Euclidean distance) to measure the similarity between feature points. By combining hash-based indexing and cascade filtering techniques, it accelerates the matching process while maintaining high accuracy. To further improve the matching accuracy, the epipolar geometry between the two images was computed based on the initial matches, and the fundamental matrix was used to optimize the matching using the RANSAC algorithm, removing outliers from the matching pairs.

2.2 Camera pose estimation and sparse reconstruction

The incremental SFM was adopted to estimate the camera pose and reconstruct the sparse point cloud of the small body (Moulon, Monasse and Marlet, 2013). Starting from an initial image pair, the fundamental matrix F is computed based on image correspondences. Using the camera intrinsic matrix K, the rotation matrix R and translation vector T between the two frames can be recovered. The initial 3D point cloud X is then reconstructed through triangulation.

New images are incrementally added, and for each newly incorporated image, the Perspective-n-Point (PnP) method is used to estimate its pose. Subsequently, Bundle Adjustment (BA) is performed for local and global optimization, ensuring optimal consistency among all camera poses and 3D points. The objective function minimizes the reprojection error, which represents the difference between the observed image points and the projected points. The optimization is formulated as follows:

$$[P, X] = argmin \sum_{i=1}^{N} \sum_{j=1}^{D} ||P_i X_j - x_j||_2^2 \quad (1)$$

Where D is the number of feature point pairs; N is the number of images; and P is the camera projection matrix, which can be calculated by the camera intrinsic matrix K, the rotation matrix R and the translation vector T ($P_i = K[R_i|T_i]$). X is the 3D coordinate of the feature point; and x is the 2D image coordinate of the feature point on the image.

2.3 Rotation axis estimation

The camera captures images while maintaining a near-hovering state. As the small body rotates, the relative positions of the camera form an approximate spatial circle, whose normal vector of the plane in which it lies can be considered as the small body’s rotation axis. The camera positions are fitted to a spatial plane. First, compute the 3D coordinates of the central point T_{mean} of all camera positions (i.e., translation vectors T) as given in Formula (2), and translate all camera positions so that the central point becomes the origin, as expressed in Formula (3).

$$T_{mean} = \frac{1}{N} \sum_{i=1}^{N} T_i \quad (2)$$

$$T_{centered} = T - T_{mean} \quad (3)$$

Then, perform Singular Value Decomposition (SVD) on the matrix $T_{centered}$, which consists of the decentralized camera positions (Formula (4)). The normal vector of the fitted plane corresponds to the third row of the right singular vector matrix V from the SVD. The normal vector of the fitted spatial plane represents the small body’s rotation axis.

$$U,\ s,\ V = SVD(T_{centered}) \quad (4)$$

$$Axis_{camera} = V[:, 2] \quad (5)$$

An additional step is required to determine its correct orientation, which should be inferred from the camera’s motion and is typically defined to align with the counterclockwise direction. Furthermore, the rotation axis obtained from SFM is initially expressed in the camera coordinate frame and must be transformed into the small body-centered J2000 inertial coordinate frame using the camera poses.

$$Axis_{j2000} = R_{j2000} \cdot Axis_{camera} \quad (6)$$

Where R_{j2000} is the camera rotation matrix at the small body-centered J2000 inertial coordinate frame; $Axis_{camera}$ is the rotation axis orientation at the camera coordinate frame after SFM; and $Axis_{j2000}$ is the rotation axis orientation at the small body-centered J2000 inertial coordinate frame.

2.4 Dense reconstruction

Dense stereo matching and point cloud fusion are applied to generate the shape model of the small body. The semi-global stereo matching algorithm is used for multi-view dense reconstruction, combining the benefits of both local and global matching to achieve a balance between accuracy and efficiency. Finally, the Poisson reconstruction method is employed to mesh

the dense point cloud, resulting in the three-dimensional surface shape model of the small celestial body.

3. Experiment data and results

We employed both simulated data and data from actual missions to validate the effectiveness of the proposed algorithm. Simulated data can provide a more flexible control over observation conditions.

3.1 Simulation platform and data

Blender software was used to generate simulated images in this study. The intrinsics of the simulation camera are shown in Table 1. The spacecraft approaches the small body from a distance of approximately 120 km, capturing 72 images over a full rotation period. During this time, the spacecraft moves less than 1 km while continuously pointing its camera at the small body. To evaluate the algorithm’s adaptability under varying observational conditions, images are simulated with different sun phase angles (The angle formed by the vectors from the small body to the Sun and from the small body to the camera) and approach angles (The angle formed by the vectors from the small body to the camera and its rotation axis orientation) by adjusting the light source position and the small body’s rotation axis orientation. A Python script automates the entire simulation process. The reference shape models include Bennu (diamond-shaped) and Itokawa (peanut-shaped), each with a diameter of approximately 500 m and occupying around 300 pixels in the images. The Bennu model, developed by (Barnouin *et al.*, 2019), is an SPC-derived version with a resolution of 0.75 m, while the Itokawa model, constructed using SPC (Gaskell *et al.*, 2008), contains over 1 million vertices.

Table 1 Simulation platform details.

Platform	Blender 3.5	
Shape model	Bennu	(Barnouin *et al.*, 2019)
	Itokawa	(Gaskell *et al.*, 2008)
Camera	Type	Perspective camera
	Focal length	628.7 mm
	Detector array size	1024 pix × 1024 pix
	Pixel size	8.5 um
	FOV	0.794° × 0.794°
Light	Sun	

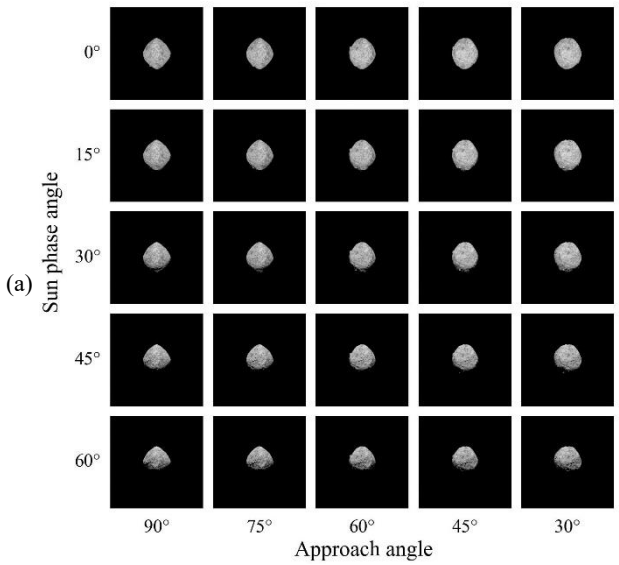

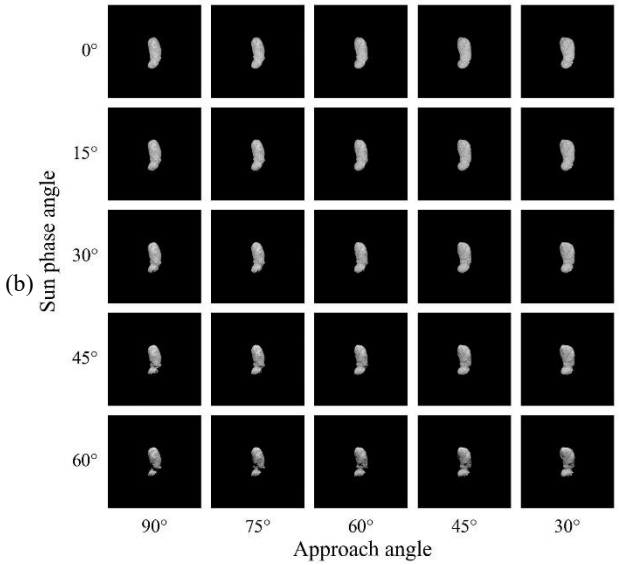

Figure 2 Simulation images of (a) Bennu and (b) Itokawa at different sun phase angle and approach angle

3.2 Experiment results on simulated data

Figure 3 shows the rotation axis estimation errors of the proposed method under different sun phase angles and approach angles. In these heatmaps, darker colors indicate larger estimation errors. The error is measured as the angle between the reference axis vector and the estimated axis vector.

The simulation results show that for the Bennu shape model, across all tested conditions with sun phase angles ranging from 0° to 60° and approach angles from 90° to 30°, the rotation axis estimation error remains below 5°, with over 80% of cases achieving errors under 3°. For the Itokawa shape model, nearly all cases yield errors below 5°, with half exhibiting errors under 3°. This difference is likely due to Bennu’s nearly spherical shape, which results in consistent imaging effects (e.g., occupied pixel count, shadow distribution). In contrast, Itokawa’s elongated and irregular shape, particularly its narrow neck, causes significant variations in imaging appearance under different illumination and viewing angles. This leads to sparse feature matches in some frames, reducing pose estimation accuracy and ultimately increasing rotation axis estimation errors.

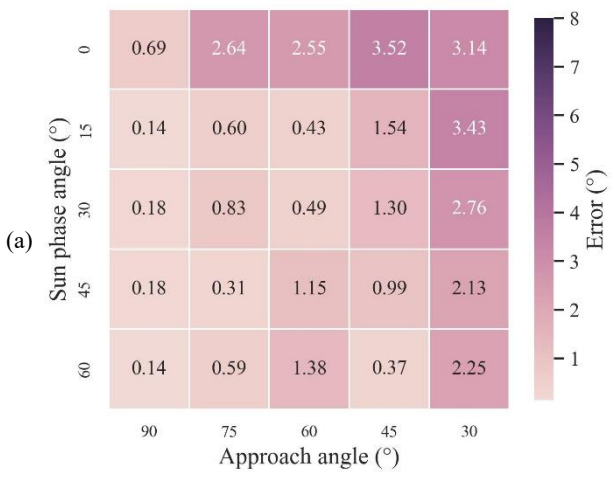

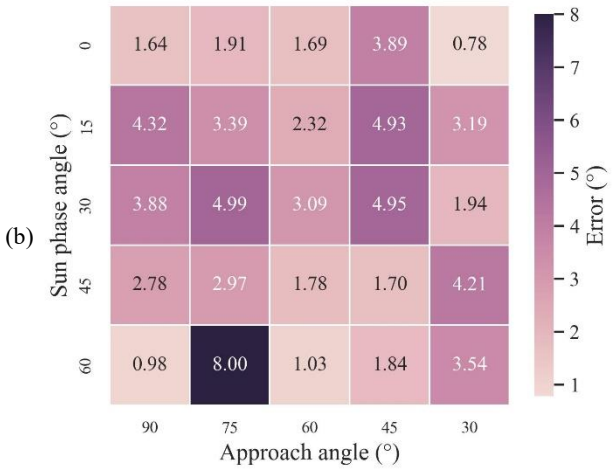

Figure 3 Estimation error of the rotation axis of the small body under different observation conditions. (a) Bennu and (b) Itokawa.

Using the Bennu shape model as an example, we further evaluated the robustness of the proposed algorithm under varying numbers of images captured within a single rotation period, in addition to different sun phase angles and approach angles. The results, presented in the cumulative frequency diagram in Figure 4, indicate that a reduction in the number of images leads to an increase in rotation axis estimation error. This effect becomes particularly pronounced when the image count is reduced to 36. Despite this, the algorithm remains highly reliable, with over 90% of cases maintaining an estimation error below 5°. These findings demonstrate the adaptability of the proposed method, even when faced with limited observational data. In addition, using these different numbers of images, the proposed method can complete the rotation axis estimation within a few minutes, demonstrating the efficiency of the method.

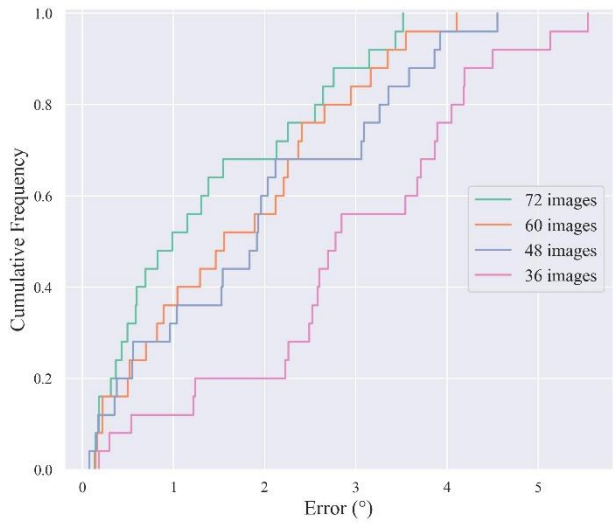

Figure 4. Cumulative frequency curve of the rotation axis estimation error when capture different numbers of images within a rotation period.

3.3 Experiment results on data from the OSIRIS-REx mission

The proposed algorithm was tested on real data captured by the OSIRIS-REx mission during its approach to Bennu. Detailed information about this dataset is provided in Table 2 and Figure 5. For the four sets of real data, the spacecraft observed Bennu from a distance of approximately 150 km, capturing 36 images within one rotation period. During this time, the sun phase angle was less than 20°, and the approach angle was about 88°, with the observation perspective nearly pointed to the equator of Bennu.

The reference rotation axis orientation of Bennu is given as (-0.03773, 0.496, -0.86751), derived from the SPC method (Barnouin and Nolan, 2021). The estimated rotation axis orientation obtained using the proposed method, along with the corresponding error, is presented in Table 3. The results show that the estimation error is approximately 1°, demonstrating the effectiveness of the proposed algorithm and its potential for application in small body exploration missions.

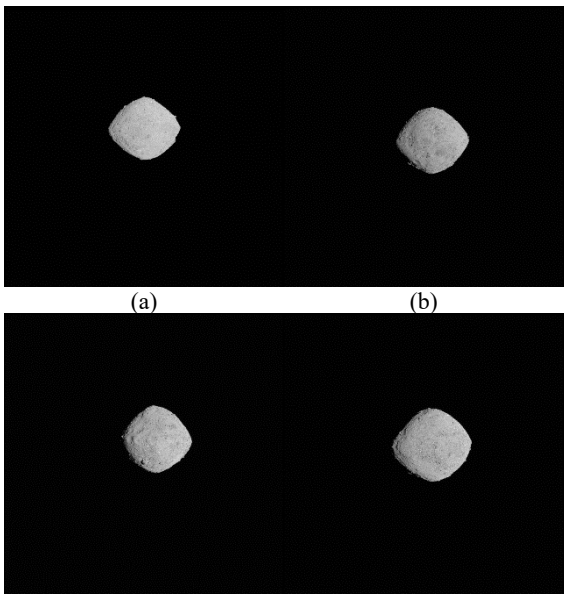

Figure 5. Real images of Bennu from the OSIRIS-REx mission. They are captured on (a) 2018-11-09, (b) 2018-11-12, (c) 2018-11-13 and (d) 2018-11-16.

Table 2. Detailed observation information of Bennu’s real images of Figure 5.

Date	Number of images	Sun phase angle	Approach angel	Distance
2018-11-09	36	~7.5°	~87.66°	~159 km
2018-11-12	36	~18°	~87.65°	~151 km
2018-11-13	36	~19°	~87.71°	~148 km
2018-11-16	36	~13.7°	~88.06°	~136 km

Table 3. Estimation results and reference values of Bennu’s rotation axis orientation.

Reference value	Ra=85.65°, Dec=-60.17°	
	0.03773, 0.49600, -0.86751	
Date	**Estimated value**	**Error (°)**
2018-11-09	0.02184, 0.51242, -0.85803	1.42
2018-11-12	0.03077, 0.49374, -0.86903	0.43
2018-11-13	0.02720, 0.49851, -0.86635	0.62
2018-11-16	0.03042, 0.50200, -0.86421	0.57

Figure 6(a) shows the reconstructed shape model using images taken on 2018-11-16, and the image resolution is about 1.85 m/pixel. Figure 6(b) is the error distribution of the

reconstructed shape model compared to the reference SPC model. The model error is defined as the distance between the vertices of the reconstructed shape model and the reference model. For each vertex, a point closest to it is found from the reference model point cloud and the Euclidean distance is calculated. In order to avoid mismatching caused by inconsistent point cloud resolution as much as possible (such as multiple reconstructed model points correspond to a reference model point, or multiple reference model points correspond to a reconstructed model point), the reference model point cloud is downsampled to the same resolution as the reconstructed model point cloud based on voxel filtering. Compared with the referenced SPC model, the constructed shape model has a maximum difference of 16.1 meters and an average difference of 2.55 meters. The areas with the large differences are mainly located around the boulder.

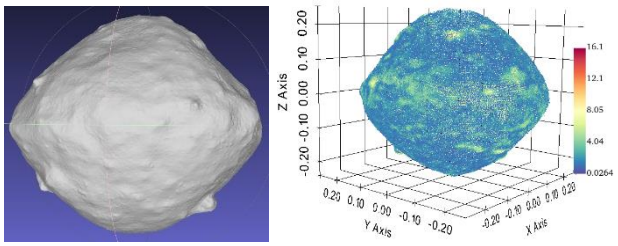

(a) (b)

Figure 6. (a) The reconstructed shape model of Bennu and (b) its error compared to the SPC model.

4. Conclusion

This paper proposes an SFM-based method for small body shape reconstruction and rotation axis estimation. The method enables fast and autonomous estimation of the shape and rotation axis of a small body at relatively large distances during the approach phase with a limited number of images. Using images captured during near-hovering observations, the relative poses of sequential images are estimated through incremental SFM. The normal vector of the plane where the fitted space circle is located is determined as the small body's rotation axis and transformed into the small body-centered J2000 inertial coordinate system. Finally, a global shape model is generated based on dense stereo matching.

The proposed method is evaluated using both simulated and real mission data. A total of 75 simulation cases are designed, considering various observational conditions such as sun phase angle, approach angle, small body shape, and the number of images captured per rotation period. The results show that over 95% of cases achieve a rotation axis estimation error below 5°. The method performs better on small bodies with regular shapes compared to those with irregular geometries. When capturing tens of images per rotation period, the rotation axis can be estimated within a few minutes, though a reduction in image count leads to increased estimation errors. Additionally, tests using four sets of OSIRIS-REx mission data for Bennu yield an estimation error of approximately 1° for its rotation axis. The dense reconstruction results show an average deviation of about 2.55 m compared to the SPC-derived shape model. These results demonstrate the effectiveness and efficiency of the proposed algorithm, proving its potential for application in small body exploration missions. Future work will focus on incorporating additional constraints into the bundle adjustment process of SFM to enhance the accuracy of rotation axis estimation and shape reconstruction.

Acknowledgements

This work was supported in part by the National Natural Science Foundation of China under Grants 42271455, 42221002, and 42325106; the Innovation Program of Shanghai Municipal Education Commission under Grant 2023ZKZD30; the Laboratory of Science and Technology on Aerospace Flight Dynamics under Grant KGJ6142210110305; and the Fundamental Research Funds for the Central Universities.

References

Bandyopadhyay, S. *et al.* (2019) ‘Silhouette-Based 3D Shape Reconstruction of a Small Body from a Spacecraft’, in *2019 IEEE Aerospace Conference*. *2019 IEEE Aerospace Conference*, Big Sky, MT, USA: IEEE, pp. 1–13. Available at: https://doi.org/10.1109/AERO.2019.8741753.

Bandyopadhyay, S. *et al.* (2021) ‘Light-robust pole-from-silhouette algorithm and visual-hull estimation for autonomous optical navigation to an unknown small body’, in. *Proc. 31st AAS/AIAA Space Flight Mechanics Meeting*, pp. 1–13.

Barnouin, O.S. *et al.* (2019) ‘Shape of (101955) Bennu indicative of a rubble pile with internal stiffness’, *Nature Geoscience*, 12(4), pp. 247–252. Available at: https://doi.org/10.1038/s41561-019-0330-x.

Barnouin, O.S. and Nolan, M.C. (2021) ‘Bennu Coordinate System Description’, *NASA Planetary Data System* [Preprint]. Available at: https://sbnarchive.psi.edu/pds4/orex/orex.mission/document/Bennu_Coordinate_System_Description.pdf.

Chamberlain, M.A., Sykes, M.V. and Esquerdo, G.A. (2007) ‘Ceres lightcurve analysis—Period determination’, *Icarus*, 188(2), pp. 451–456. Available at: https://doi.org/10.1016/j.icarus.2006.11.025.

Gaskell, R.W. *et al.* (2008) ‘Gaskell itokawa shape model v1. 0’, *NASA Planetary Data System*, p. HAY-A.

Lowe, D.G. (2004) ‘Distinctive Image Features from Scale-Invariant Keypoints’, *International Journal of Computer Vision*, 60(2), pp. 91–110. Available at: https://doi.org/10.1023/B:VISI.0000029664.99615.94.

Mottola, S. *et al.* (2014) ‘The rotation state of 67P/Churyumov-Gerasimenko from approach observations with the OSIRIS cameras on Rosetta’, *Astronomy & Astrophysics*, 569, p. L2. Available at: https://doi.org/10.1051/0004-6361/201424590.

Moulon, P., Monasse, P. and Marlet, R. (2013) ‘Global Fusion of Relative Motions for Robust, Accurate and Scalable Structure from Motion’, in *2013 IEEE International Conference on Computer Vision*. *2013 IEEE International Conference on Computer Vision (ICCV)*, Sydney, Australia: IEEE, pp. 3248–3255. Available at: https://doi.org/10.1109/ICCV.2013.403.

Muinonen, K. *et al.* (2015) ‘Asteroid lightcurve inversion with Lommel–Seeliger ellipsoids’, *Planetary and Space Science*, 118, pp. 227–241. Available at: https://doi.org/10.1016/j.pss.2015.09.005.

Panicucci, P. *et al.* (2023) ‘Vision-based estimation of small body rotational state’, *Acta Astronautica*, 213, pp. 177–196. Available at: https://doi.org/10.1016/j.actaastro.2023.08.046.

Park, R.S. *et al.* (2019) ‘High-resolution shape model of Ceres from stereophotoclinometry using Dawn Imaging Data’, *Icarus*, 319, pp. 812–827. Available at: https://doi.org/10.1016/j.icarus.2018.10.024.

Preusker, F. *et al.* (2015) ‘Shape model, reference system definition, and cartographic mapping standards for comet 67P/Churyumov-Gerasimenko – Stereo-photogrammetric analysis of Rosetta/OSIRIS image data’, *Astronomy & Astrophysics*, 583, p. A33. Available at: https://doi.org/10.1051/0004-6361/201526349.

Zhang, T., Xu, K. and Ding, X. (2021) ‘China’s ambitions and challenges for asteroid–comet exploration’, *Nature Astronomy*, 5(8), pp. 730–731. Available at: https://doi.org/10.1038/s41550-021-01418-9.